Received: 7 January 2020 | Revised: 24 February 2020 | Accepted: 25 February 2020

DOI: 10.1002/chir.23216

WILEY

SPECIAL ISSUE ARTICLE

Pressure dependence of vibrational optical activity of model biomolecules. A computational study

Luboš Plamitzer[1,2] | **Petr Bouř**[1]

[1]Institute of Organic Chemistry and Biochemistry, Czech Academy of Sciences, Flemingovo náměstí 542/2, Prague 6, 166 10, Czech Republic

[2]Faculty of Mathematics and Physics, Charles University, Ke Karlovu 2027/3, Prague 2, 121 16, Czech Republic

Correspondence
Petr Bouř, Institute of Organic Chemistry and Biochemistry, Czech Academy of Sciences, Flemingovo náměstí 542/2, Prague 6, 166 10. Czech Republic.
Email: bour@uochb.cas.cz

Funding information
Grantová Agentura České Republiky, Grant/Award Number: 18-05770S; Ministry of Education of the Czech Republic, Grant/Award Numbers: e-INFRA LM2018140, LTC17012, CZ.02.1.01/0.0/0.0/16_019/0000729

Abstract

Change of molecular properties with pressure is an attracting means to regulate molecular reactivity or biological activity. However, the effect is usually small and so far explored rather scarcely. To obtain a deeper insight and estimate the sensitivity of vibrational optical activity spectra to pressure-induced conformational changes, we investigate small model molecules. The Ala-Ala dipeptide, isomaltose disaccharide and adenine-uracil dinucleotide were chosen to represent three different biomolecular classes.

The pressure effects were modeled by molecular dynamics and density functional theory simulations. The dinucleotide was found to be the most sensitive to the pressure, whereas for the disaccharide the smallest changes are predicted. Pressure-induced relative intensity changes in vibrational circular dichroism and Raman optical activity spectra are predicted to be 2–3-times larger than for non-polarized IR and Raman techniques.

KEYWORDS

density functional theory, high pressure, molecular dynamics, spectra simulations, vibrational optical activity

1 | INTRODUCTION

Experimentally, effects of pressures up to about 1 GPa on the conformation of biologically relevant molecules have been studied for a long time. Pressure-induced coagulation of egg white was described already in 1914.[1] Most studies targeted proteins, whereas less attention has been paid to other systems, such as nucleic acids and polysaccharides.

For proteins, the pressure variation can be used to characterize partially or completely unfolded protein species.[2,3] Some applications involve protein–protein interactions, their volumetric properties,[4-6] or kinetics of fibril growth, including recPrP or α-synuclein.[7-11]

The mechanism of pressure-induced changes in proteins has been described in terms of volume reduction, water penetration to cavities, or hydration of hydrophobic residues.[12-22] The effects of entropy and structure of the solvent have also been discussed.[23] High pressure may both stabilize and destabilize conformers, and may affect long and short peptide chains differently.[24,25] The pressure effects were conveniently modeled by molecular dynamics, with typical trial proteins including ubiquitin, BPTI, lysozyme and myoglobin.[4,5,26-33]

Polysaccharide high pressure studies dealt mostly with physicochemical and morphological properties of starches. Their viscosity or solubility can vary; they can form a gel, or both the secondary and tertiary structures can irreversibly change due to the pressure.[34-40] Typical pressures used were 200–600 MPa.[34] For example, the pressure resistance was found to be proportional to the amylopectin content, and differed for A, B and C-type starches.[35,38] Saccharide-protein systems have been investigated as well.[41,42] However, we could

[This article is part of the Special Issue: Proceedings from 31st International symposium on Chirality.]

not find any computational studies on pressure effects in saccharides.

For DNA, elevated pressure induced the B/Z conformational change[43,44] and affected stability of non-canonical structures (G-quadruplex and i-motif).[45-47] Such changes were found to be strongly dependent on the sequence and solvent.[48-50] Similar observations were reported for RNA.[51] Studied nucleic acid forms included RNA and DNA hairpins,[52,53] and tRNA.[54,55] Some effects were modeled by molecular dynamics (MD).[56] For tRNA, due to its inefficient packing, unfolding characteristic was found to differ from that of DNA or proteins.[55]

The pressure-induced structural changes were monitored by NMR,[2,15,16,57-59] Raman, IR,[7,60,61] and circular dichroism.[62,63] Raman optical activity (ROA) and vibrational circular dichroism (VCD) have not been used, even though they are in general quite sensitive to changes in molecular geometry.[22] Therefore, in the present study, we focus on these to forms of vibrational optical activity. We also feel that previous theoretical simulations of proteins under high pressure lack a systematic approach. At least in one case we could not reproduce some results from earlier molecular dynamics studies.

We thus focus on computational methodology used to simulate the conformational changes induced by the pressure, and their potential monitoring by ROA and VCD spectra. For the sake of converged and reliable simulations, small molecules are used, at least formally representing three common classes of biopolymers – the Ala-Ala dipeptide ("protein"), isomaltose ("starch") and A-U dinucleotide ("DNA/RNA"). The isomaltose contains an α-(1–6)-linkage, mimicking the glycosidic bond in amylopectins.

As shown below, the simulations confirm the importance of the choice of the water model, as indicated before.[30,64,65] We also found that relatively large simulation times were needed for good reproducibility of the results because the pressure effects are relatively small compared to statistical fluctuations during the MD run. As expected, the chiroptical ROA and VCD methods are predicted to be more sensitive to the pressure-induced changes than their unpolarized analogues (Raman, IR). We thus hope that our results will provide guidance for future computations and experiments, and will lead to a better control of biomolecular behavior under elevated pressure.

2 | METHODS

Studied molecules (Figure 1) were prepared with tools provided by Amber 18[66] (tleap, NAB) and GLYCAM Web

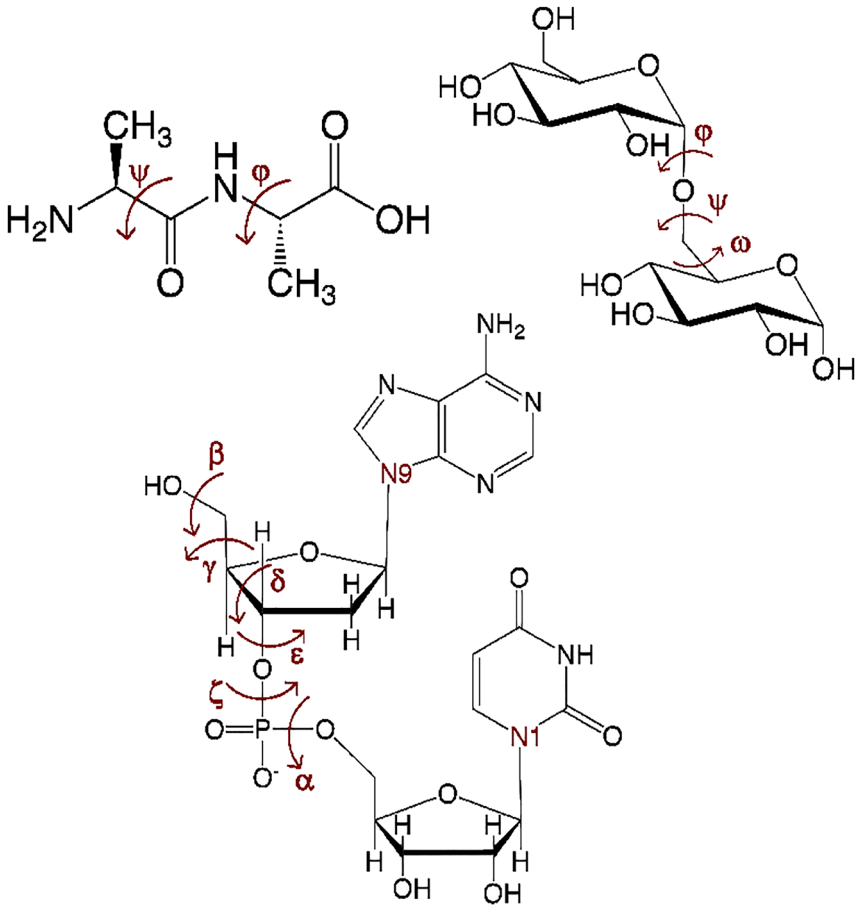

FIGURE 1 Studied molecules: Ala-Ala dipeptide (top left), isomaltose (top right) and A-U dinucleotide (bottom). Dihedral angles most characteristic for longer polymers are indicated

(Carbohydrate Builder),[67] using the ff14SB (Ala-Ala),[68] OL3 (A-U)[69,70] and Glycam06 force fields.[71] The molecules were solvated in a rectangular box with TIP3P (Ala-Ala, isomaltose, A-U), TIP4P, TIP5P and SPCFW (Ala-Ala only) force fields for water.

To monitor conformer populations, the weighted histogram analysis method (WHAM)[72] was used for Ala-Ala, with respect to dihedral angles φ (C-N-C_α-C) and ψ (N-C_α-C-N). Unrestrained (free) MD proved to be more practical for isomaltose, where dihedral angles φ (O-C1-O6-C6), ψ (C1-O6-C6-C5) and ω (O6-C6-C5-O) were monitored. Similarly for A-U with 6 characteristic dihedral angles, α, β, γ, δ, ε and ζ,[73] we used a free dynamics and conformer classes based on the N1(U)-N9(A) atomic distance only.

The simulations were performed using the pmemd (Ala-Ala) and pmemd.cuda (isomaltose, A-U) Amber modules. For the free MD runs, system geometries were minimized (steepest descent followed by conjugate gradient), warmed up (0 to 300 K, 20 ps, NVT), equilibrated (100 ps, NVT; 200 ps, NpT), and subjected to a production run (300 K, ~1 μs, NpT, 2 fs integration step). Pressures of 1 bar, 4 kbar and 8 kbar were maintained with the Monte Carlo barostat,[74] the temperature was kept constant with the Langevin thermostat.[75]

For the WHAM simulation, (φ, ψ) grid with 20 degree increments and a force constant of 25 kcal mol^{-1} rad^{-2} were used. At each grid point, minimization, heating and two-step equilibration (NVT, NpT) were followed by a production run (300 K, 4 ns, NpT, 1–2 fs integration step depending on the employed water model).

IR, VCD, Raman and ROA spectra were generated using the Gaussian 16 program[76] and the B3LYP[77]/6–311++G**/GD3BJ[78]/CPCM[79] approximation level. For Ala-Ala, the spectra were averaged from 100 MD snapshots for each conformer class, following the method in ref. 80. For the other two molecules only the typical conformation (MD snapshot) for each conformer class was selected, using Amber CPPTRAJ clustering tools.[81] A constrained normal mode partial optimization was used[82-84] to preserve the MD geometries and relax higher-frequency vibrational motions. Finally, the spectra of conformers were combined using populations predicted for different pressures by MD. A dimensionless spectral variation was calculated from the spectra predicted for 1 bar (S_0) and 8 kbar (S_p),

$$\delta = \frac{\int |S_p - S_0| d\omega}{\int |S_0| d\omega}, \quad (1)$$

which proved to be useful in the spectra comparison, apart from a visual inspection. The upper pressure limit (8 kbar) was chosen with respect to values expected in common experiments.

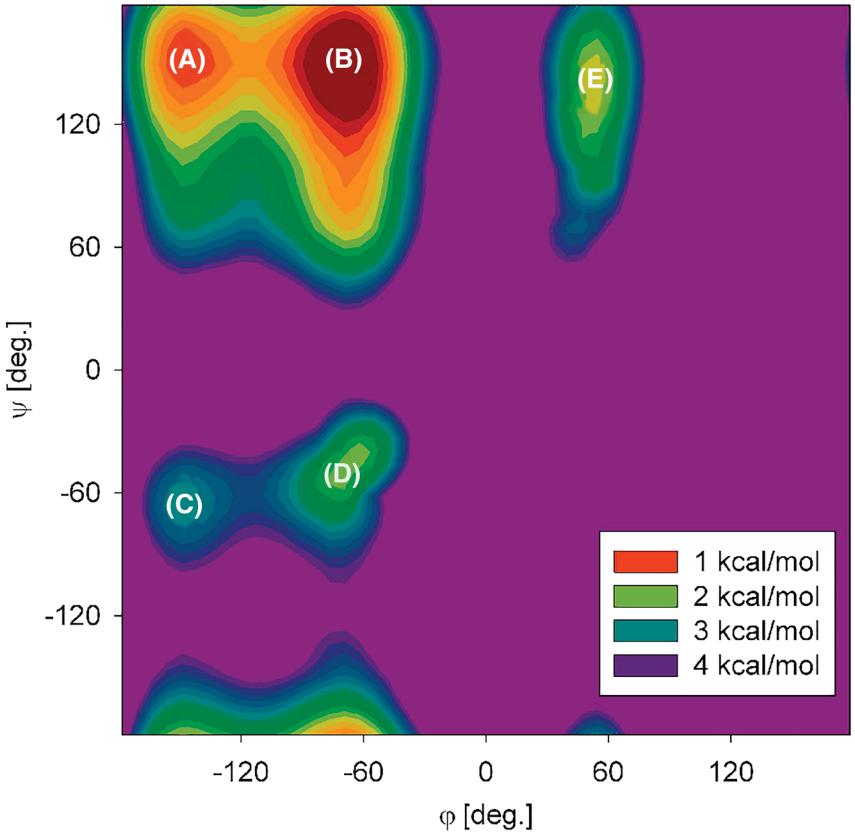

FIGURE 2 Ramachandran plot, i.e., the dependence of free energy on the (φ, ψ) torsion angles, as obtained by WHAM for zwitterionic Ala-Ala (1 bar, SPCFW water model)

3 | RESULTS AND DISCUSSION

3.1 | Dipeptide MD

The Ala-Ala MD was run with the SPCFW, TIP3P, TIP4P and TIP5P water force fields,[85] because previous works suggest that the water model can alter helical stability,[86] preference for folded vs. unfolded state,[87] and the structure of the solvation shell.[88] Obtained potential energy surface is plotted in Figure 2. We divided Ala-Ala conformers into five conformer classes (A-E); their populations for various water force fields and three pressures are plotted in Figure 3.

Although the trends in conformer populations are more or less consistently predicted with all the force fields, detailed distributions differ. When the pressure is increased from 1 bar to 4 kbar, conformer B always becomes more populated. This conformer corresponds to the polyproline II (PP_{II}), structure, often associated with so called random conformation of proteins and peptides.[89] However, further increase to 8 kbar results in a higher population of B only for the TIP4P force field. Population of the A conformer (close to the β-sheet protein geometry[90]) decreases approximately linearly with increasing pressure, regardless of the water model employed. Geometry of the D conformer is close to normal protein α-helix, while the E structure would correspond to the left-handed α-helix.[90] The C and D conformer populations do not seem to be affected by the pressure, while population of E grows. At 8 kbar the SPCFW, TIP3P and TIP5P force fields indicate that this left-handed "helix" is even more populated than the right-handed one.

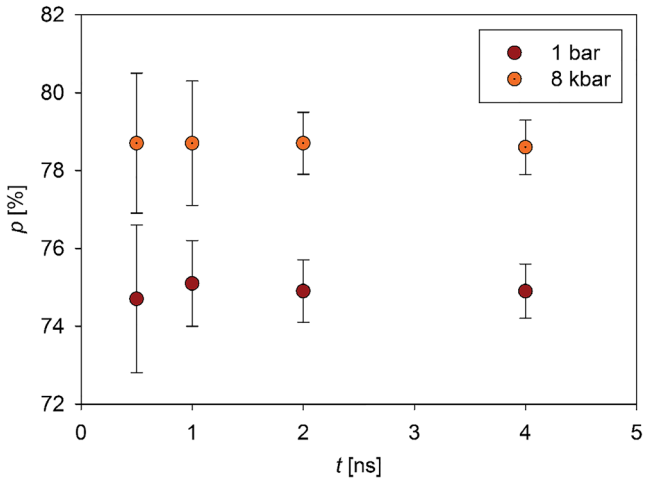

FIGURE 4 Dependence of the Ala-Ala B conformer population and 99% confidence intervals (errors) on the simulation time, for the SPCFW water force field, and WHAM simulations under 1 bar and 8 kbar

A more detailed look at the Ramachandran plot revealed that geometries of the minima also slightly change. For example, the equilibrium value of the φ angle in conformer B increased by about 3° for 8 kbar. A consequence for the spectra would be difficult to simulate with the

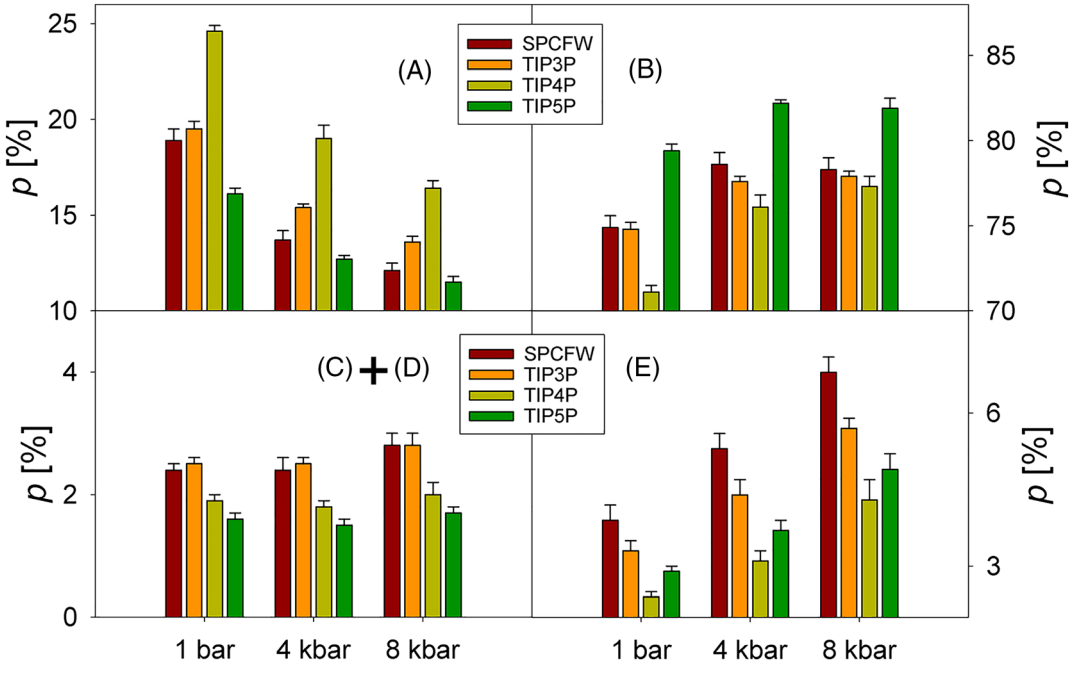

FIGURE 3 Populations (%) of the Ala-Ala conformer classes (A, B, C + D, E) for three pressures, as obtained with four different water force fields (SPCFW, TIP3P, TIP4P, TIP5P)

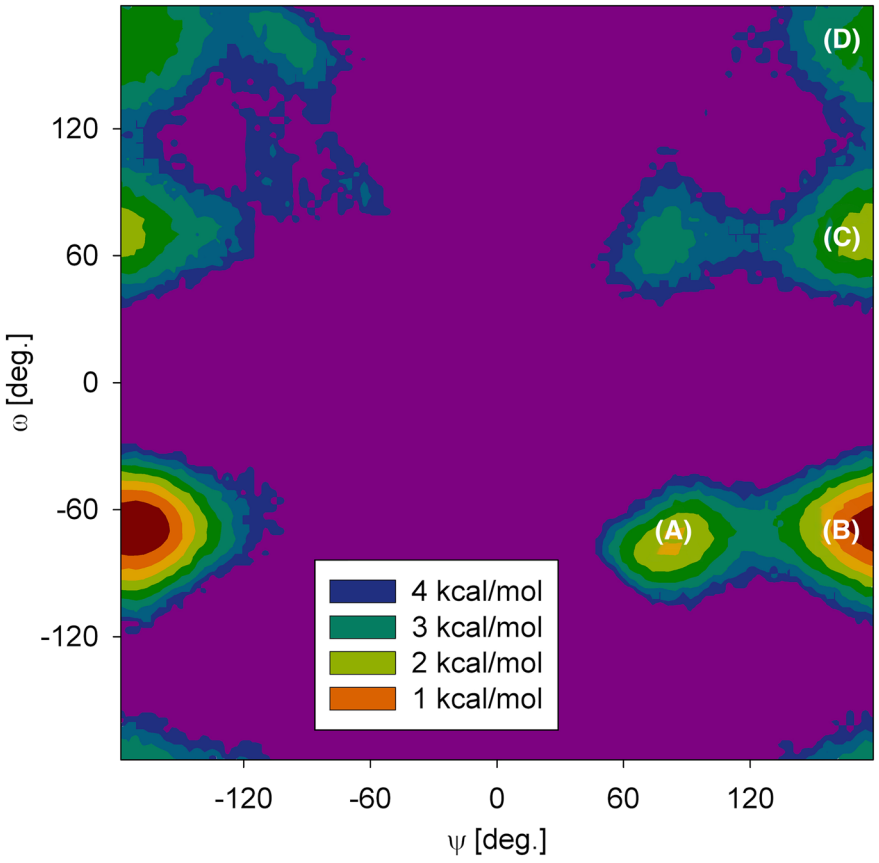

FIGURE 5 Dependence of isomaltose free energy on the (ψ, ω) angles (free MD, 1 bar)

present computational methodology (much more snapshots and different optimization scheme might be required). Nevertheless, we estimate that for the selected molecules these effects are less significant than those caused by the changes in conformer populations.

An error analysis indicated the importance of running sufficiently long MD simulations. Otherwise the predicted population changes under different pressures were smaller than statistical fluctuations of MD. Figure 4 shows a gradual decrease of the 99% confidence interval for the 1 bar and 8 kbar SPCFW populations. Within 0.5–2 ns the formal error gets smaller to about one half, but further prolongation to 4 ns causes only marginal improvement in the accuracy. The graphs suggest that the resultant error in conformer populations is smaller than 1%.

In general, the MD results are in agreement with previous studies on Ala-Ala,[91,92] which were, however, typically focused on the effect of the protein force field and not that of the pressure.[93]

TABLE 1 Populations and their standard deviations (%) of isomaltose conformers for three pressures

Pressure	A	B	C	D
1 bar	6.5 ± 0.3	74.2 ± 0.9	8.7 ± 0.3	8.5 ± 0.9
4 kbar	7.6 ± 0.1	71.5 ± 2.7	9.5 ± 0.7	9.4 ± 1.8
8 kbar	6.8 ± 0.7	69.5 ± 1.4	10.0 ± 1.0	10.2 ± 0.7

3.2 | Disaccharide MD

Because the φ angle stayed close to 70° and did not much depend on the pressure in all MD simulations, we focused on the behavior of the other two (ψ and ω)

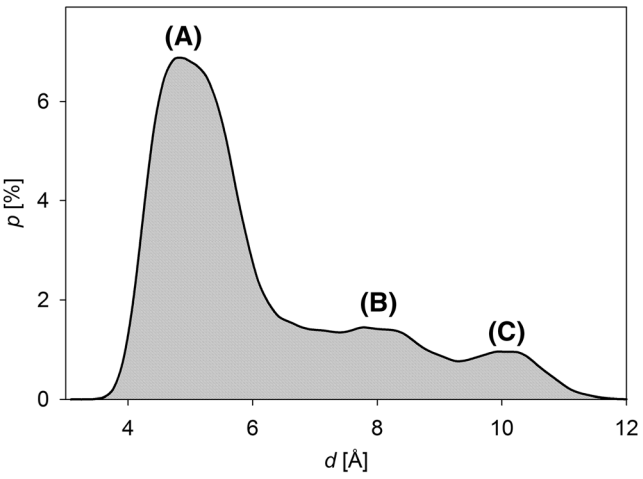

FIGURE 6 A–U, probability distribution with respect to the N1(U) - N9(A) distance

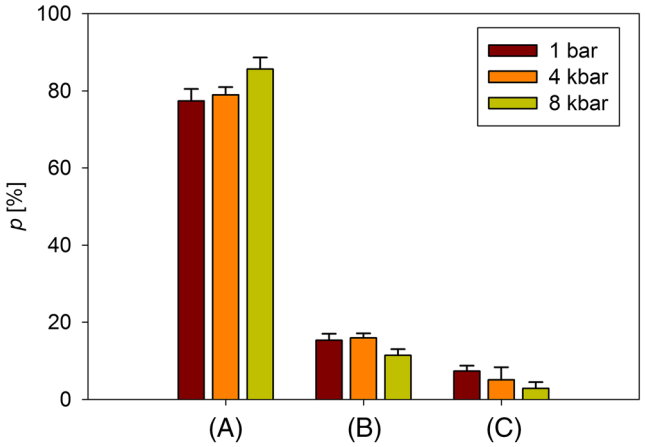

FIGURE 7 Populations of the A-U conformers calculated for the three pressures

TABLE 2 Computed molecular volumes (bohr^3) for Ala-Ala, isomaltose and A-U conformers

Conformer	Ala-Ala	Isomaltose	A-U
A	1395	2506	3703
B	1419	2671	3966
C	1490	2411	4056
D	1167	2578	-
E	1483	-	-

torsion angles. The dependence of the free energy on them for 1 bar is plotted in Figure 5. Four distinct conformers (A-D) can be identified, their populations for different pressures are summarized in Table 1.

Clearly, population of A remains nearly stable, while bigger changes occur for the other conformers. C and D become slightly more populated under higher pressures, and the biggest change is predicted for B, losing 5% in the 1 bar → 8 kbar pressure change. Overall, these changes are quite minor and sometimes comparable with the errors, which were calculated from ensemble of three unrestrained simulations with different starting velocities, each 750 ns long.

3.3 | Dinucleotide MD

The MD geometries were sorted into three conformer classes (A, B and C), using a hierarchical agglomerative clustering algorithm based on the distance between uracil and adenine atoms (N1 and N9, see Figure 1). A distance-dependent probability density (integrating to one over all distances) is plotted in Figure 6. Integrated populations obtained for three pressures are plotted in Figure 7.

The population of the most compact conformer A (with the two nitrogen atoms closest to each other,

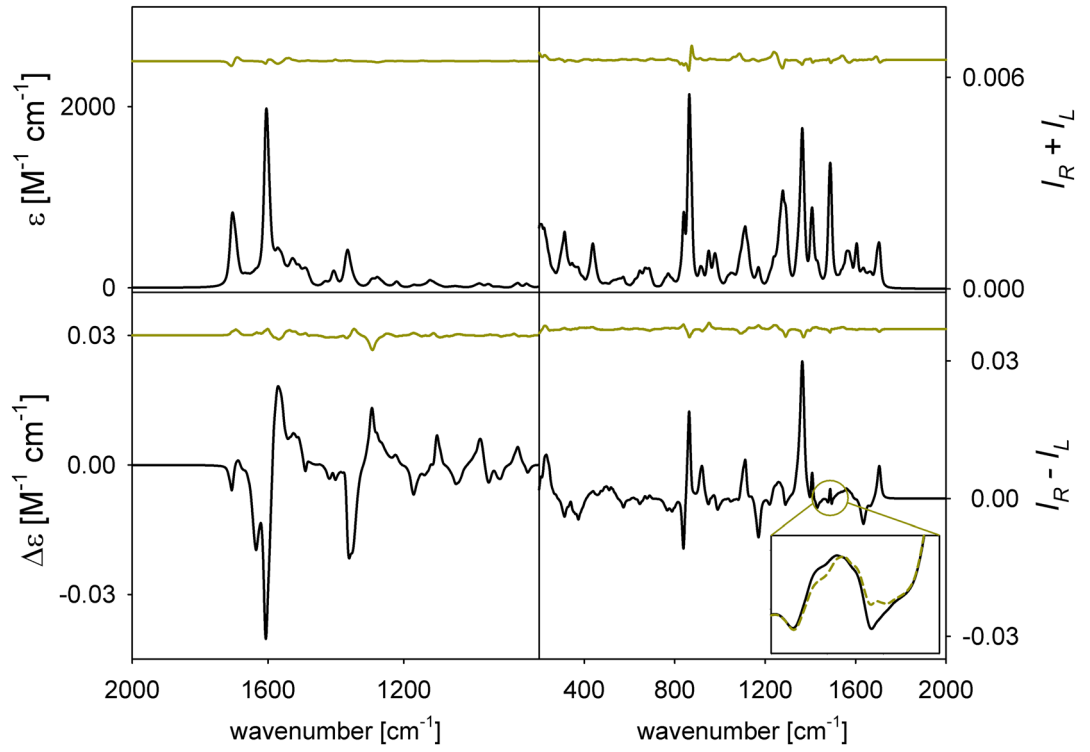

FIGURE 8 Simulated IR (ε), VCD (Δε), Raman ($I_R + I_L$) and ROA ($I_R - I_L$) spectra of Ala-Ala, and the difference S_0 (1 bar) - S_p (8 kbar), green line, caused by the pressure. An example of ROA at the normal (solid black) and elevated (green dashed line) pressure is shown in the inset

d ~ 5 Å) increases by 8%, with the biggest change occurring between 4 and 8 kbar (6.5%). Populations of B and C decrease, with the latter almost vanishing at 8 kbar. The errors and confidence intervals were calculated from ensemble of three unrestrained simulations, each 1 μs long, but with different initial velocities.

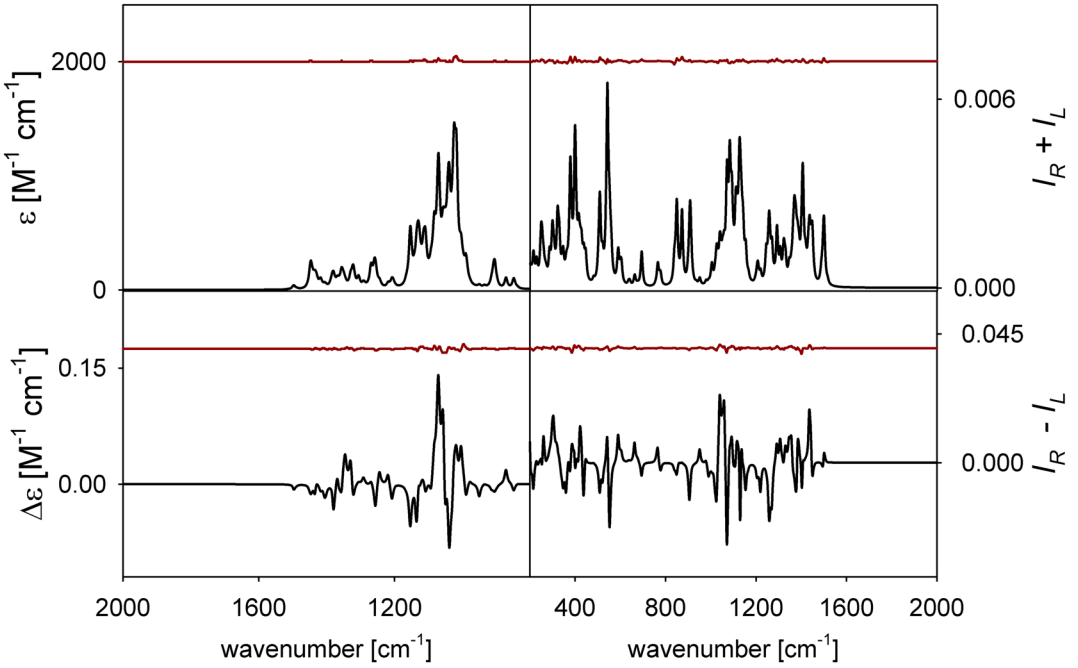

FIGURE 9 As in Figure 8, for isomaltose, S_0 - S_p in red

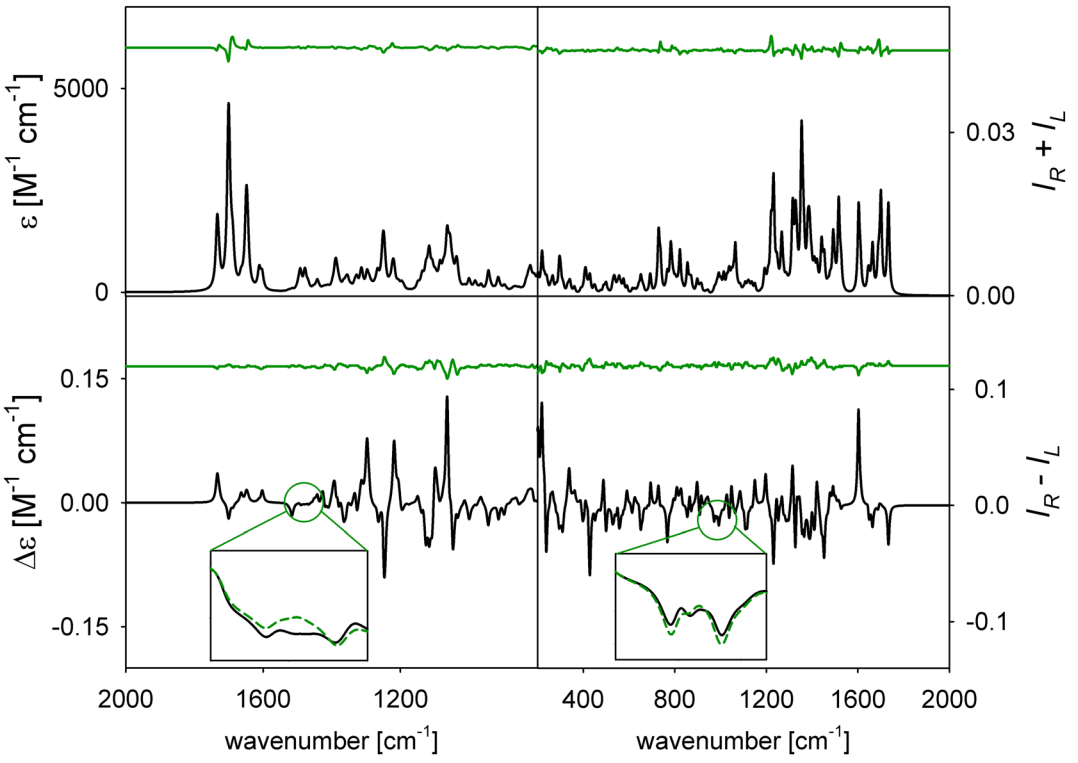

FIGURE 10 As in Figure 8, for the A-U dinucleotide

3.4 | Molecular volumes

Molecular volumes were calculated using the Gaussian 16 algorithm.[76] As predicted earlier, an increase in the pressure should favor species with smaller volumes.[61] This is more or less confirmed by the calculated volumes (V) summarized in Table 2, where at least isomaltose and the A-U dinucleotide follow this trend. Populations of the most voluminous conformers (B of isomaltose, $V \approx 2671$ bohr^3,and C of A-U, $V \approx 4056$ bohr^3) decrease with the pressure. For Ala-Ala, the differences between volumes of individual conformers are very small (below the computational error of ~100 bohr^3, according to the Gaussian 16 manual) and other factors probably prevail.

TABLE 3 Predicted integrated spectral variation under the pressure (δ, in %) for all studied molecules and spectroscopic techniques

Spectroscopy	Ala-Ala	Isomaltose	A-U
IR	4	2	5
VCD	8	5	15
Raman	4	2	5
ROA	9	6	9

3.5 | Optical spectra

IR, VCD, Raman and ROA spectra together with changes caused by the 1 bar → 8 kbar pressure surge, as predicted by MD and DFT, are plotted in Figures 8–10. Clearly, the changes are quite minor, typically within 10% of the average intensity. The changes are about comparable for Ala-Ala and A-U, but much smaller for isomaltose. Only in a few specific cases of ROA and VCD, more pronounced differences can be observed. Typically, the relative

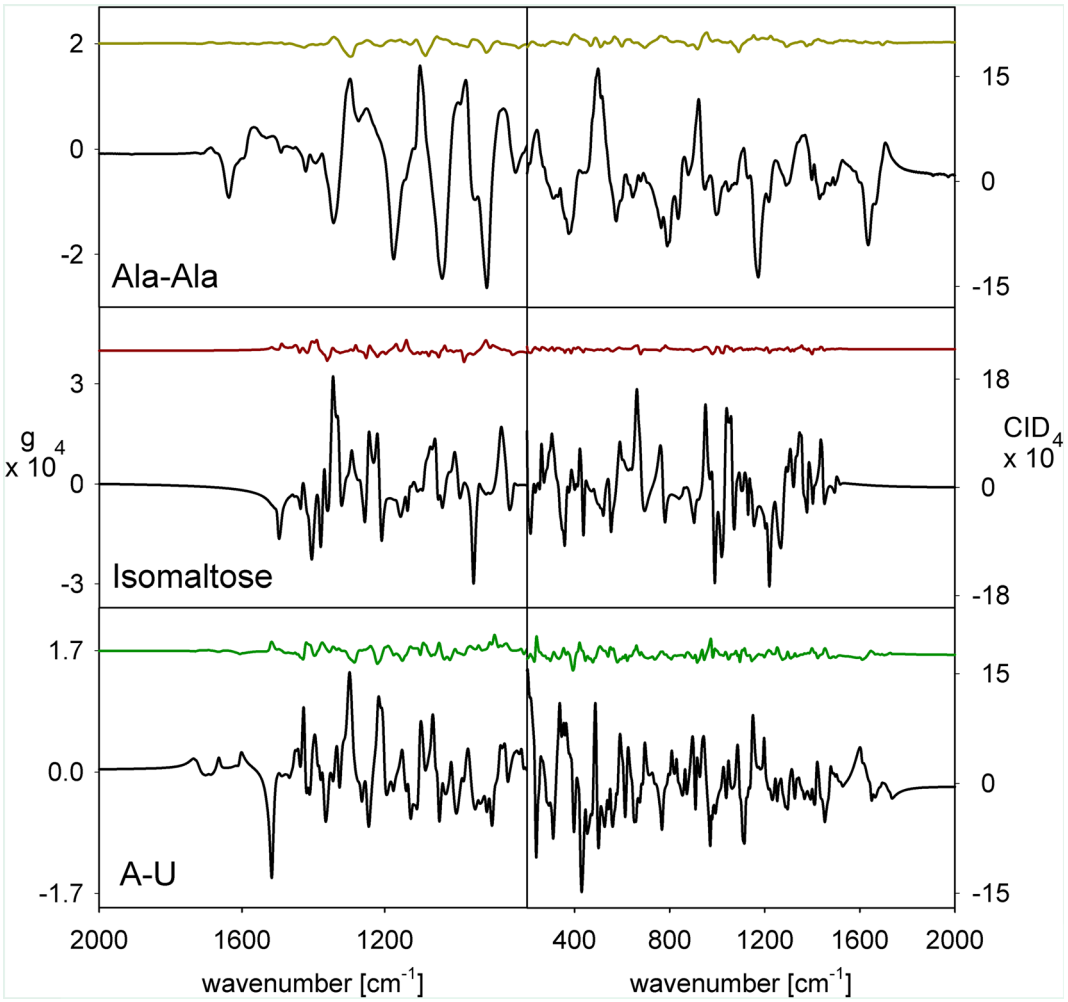

FIGURE 11 Simulated dissymmetry factors (left) and CID ratios (right) for the three studied molecules, and their pressure-induced changes (in colors)

changes are bigger for spectral regions with small intensities. Examples of such regions are magnified in the insets of Figures 8 and 10.

For IR, the largest changes accompany the largest intensities of the amide I and II modes (Figure 8, Ala-Ala, within about 1600–1700 cm^{-1}) and carboxyl stretching (Figure 10, A-U, also around 1650 cm^{-1}). Interestingly, the largest VCD changes occur in a different lower-frequency region than IR, dominated by more delocalized vibrations. This somewhat contrasts with the Raman and ROA spectra, where the changes are spread more evenly, although the most susceptible Raman bands do not automatically coincide with the most sensitive ROA signals.

For Ala-Ala, different water force fields provided spectra differing by about 10% in intensity, the changes caused by the pressure were nearly the same (not shown). Frequency shifts induced by the pressure were reported in the literature as well,[94] however, these are not well captured by the present simulations focused on the conformational dependence only. For example, bond lengths and distances between atoms of different molecules in the clusters are allowed to change in our optimization protocol, which might affect frequencies of some vibrational bands.

The predicted spectral variations (δ, eq. 1) are listed in Table 3. This parameter can be thought of as a measure of the sensitivity to the pressure. As can be seen in the table, the chiroptical techniques (VCD and ROA) are about 2–3-times more sensitive than their unpolarized analogs (IR, Raman). There is a little difference between VCD and ROA, except for A-U, where VCD is predicted to be ~1.7× more sensitive.

A similar picture is provided by the dissymmetry factors $g = \Delta\varepsilon/\varepsilon$ and circular intensity differences $CID = (I_R - I_L)/(I_R + I_L)$ plotted in Figure 11. One can see that the relative pressure-induced changes of these two variables are somewhat larger than for the other spectra. For example, while ROA and VCD isomaltose intensities change less than by 4% within 1 bar - 8 kbar, more than 8% change can often be seen in g or CID. This, however, does not make eventual experimental observation easier, because large g/CID factors are often seen in weak bands that are difficult to measure.

3.6 | Experimental aspects

Measurements of high-pressure VCD and ROA spectra go beyond the scope of this work, nevertheless it is clear that the experiments may be quite difficult, at least for the small molecules. Technical difficulties include a very small amount of the sample in the usual diamond cell (nanoliters) from which the signal must be obtained, polarization artifacts caused by the diamond, etc. The conformational changes may also be masked by other effects, such as the aforementioned changes in vibrational frequencies,[94] which were not properly included in the present study. Some advantage might be possibly gained by the higher pressures accessible in optical experiments (up to hundreds of GPa), as compared to the NMR detection (0.2–0.4 GPa).[95]

4 | CONCLUSION

We conducted a thorough computational study of three model systems chosen to represent biologically important molecules – proteins, nucleic acid polymers and polysaccharides. Within the molecular dynamics modeling the pressure-induced conformational changes could be predicted and the computational error estimated. Relatively long times were needed for reliable predictions, which may explain some problems with similar simulations encountered in the previous studies on larger systems.

The 1 bar → 8 kbar pressure hike caused minor variations in conformer populations, typically up to ~10%. For bigger molecules more significant changes may be expected, nevertheless, already our miniseries indicated that different molecules exhibit significantly different sensitivity to the pressure. For example, the disaccharide was rather indifferent to it, which might explain the absence of relevant experimental data for similar molecules in the literature. Various water force fields provided similar results with respect to the pressure sensitivity, although they differed in absolute conformer populations. Molecular volume was confirmed as an important indicator of the pressure sensitivity.

VCD and ROA intensities were readily found more sensitive to the pressure than IR and Raman spectroscopies. Although actual measurements might be quite problematic, we hope that the present study can provide useful guidance to them.

ACKNOWLEDGMENTS

The work was supported by the Grant Agency (18-05770S) and Ministry of Education of the Czech Republic (e-INFRA LM2018140, LTC17012, and CZ.02.1.01/0.0/0.0/16_019/0000729).

ORCID

Luboš Plamitzer https://orcid.org/0000-0001-8389-9186
Petr Bouř https://orcid.org/0000-0001-8469-1686

REFERENCES AND NOTES

1. Bridgman PW. The coagulation of albumen by pressure. *J Biol Chem*. 1914;19:511-512.
2. Kitahara R, Akasaka K. Close identity of a pressure-stabilized intermediate with a kinetic intermediate in protein folding. *P Natl Acad Sci USA*. 2003;100(6):3167-3172.
3. Smeller L, Rubens P, Heremans K. Pressure effect on the temperature-induced unfolding and tendency to aggregate of myoglobin. *Biochem US*. 1999;38(12):3816-3820.
4. Paci E, Marchi M. Intrinsic compressibility and volume compression in solvated proteins by molecular dynamics simulation at high pressure. *P Natl Acad Sci USA*. 1996;93(21):11609-11614.
5. Ploetz EA, Smith PE. Simulated pressure denaturation thermodynamics of ubiquitin. *Biophys Chem*. 2017;231:135-145.
6. Marchal S, Torrent J, Masson P, et al. The powerful high pressure tool for protein conformational studies. *Braz J Med Biol Res*. 2005;38(8):1175-1183.
7. Cordeiro Y, Foguel D, Silva JL. Pressure-temperature folding landscape in proteins involved in neurodegenerative diseases and cancer. *Biophys Chem*. 2013;183:9-18.
8. Meersman F, Dobson CM, Heremans K. Protein unfolding, amyloid fibril formation and configurational energy landscapes under high pressure conditions. *Chem Soc Rev*. 2006;35(10):908-917.
9. Torrent J, Martin D, Igel-Egalon A, Beringue V, Rezaei H. High-pressure response of amyloid folds. *Viruses*. 2019;11(3):202.
10. Piccirilli F, Plotegher N, Spinozzi F, et al. Pressure effects on alpha-synuclein amyloid fibrils: an experimental investigation on their dissociation and reversible nature. *Arch Biochem Biophys*. 2017;627:46-55.
11. Piccirilli F, Plotegher N, Ortore MG, et al. High-pressure-driven reversible dissociation of alpha-synuclein fibrils reveals structural hierarchy. *Biophys J*. 2017;113(8):1685-1696.
12. Hillson N, Onuchic JN, García AE. Pressure-induced protein-folding/unfolding kinetics. *P Natl Acad Sci USA*. 1999;96(26):14848-14853.
13. Roche J, Caro JA, Norberto DR, et al. Cavities determine the pressure unfolding of proteins. *P Natl Acad Sci USA*. 2012;109(18):6945-6950.
14. Hummer G, Garde S, García AE, Paulaitis ME, Pratt LR. The pressure dependence of hydrophobic interactions is consistent with the observed pressure denaturation of proteins. *P Natl Acad Sci USA*. 1998;95(4):1552-1555.
15. La Penna G, Mori Y, Kitahara R, Akasaka K, Okamoto Y. Modeling (15)N NMR chemical shift changes in protein backbone with pressure. *J Chem Phys*. 2016;145(8):085104.
16. Day R, García AE. Water penetration in the low and high pressure native states of ubiquitin. *Proteins*. 2007;70(4):1175-1184.
17. Chen CR, Makhatadze GI. Molecular determinant of the effects of hydrostatic pressure on protein folding stability. *Nat Commun*. 2017;8(1):14561.
18. Marques MI, Borreguero JM, Stanley HE, Dokholyan NV. Possible mechanism for cold denaturation of proteins at high pressure. *Phys Rev Lett*. 2003;91(13):138103.
19. Dias CL. Unifying microscopic mechanism for pressure and cold denaturations of proteins. *Phys Rev Lett*. 2012;109(4):048104.
20. Royer CA. Revisiting volume changes in pressure-induced protein unfolding. *Biochim Biophys Acta*. 2002;1595(1–2):201-209.
21. Grigera JR, McCarthy AN. The behavior of the hydrophobic effect under pressure and protein denaturation. *Biophys J*. 2010;98(8):1626-1631.
22. Refaee M, Tezuka T, Akasaka K, Williamson MP. Pressure-dependent changes in the solution structure of hen egg-white lysozyme. *J Mol Biol*. 2003;327(4):857-865.
23. Harano Y, Yoshidome T, Kinoshita M. Molecular mechanism of pressure denaturation of proteins. *J Chem Phys*. 2008;129(14):145103.
24. Yoshidome T, Kinoshita M. Pressure effect on helix–coil transition of an alanine-based peptide: theoretical analysis. *Chem Phys Lett*. 2009;477(1–3):211-215.
25. Mori Y, Okumura H. Molecular dynamics of the structural changes of helical peptides induced by pressure. *Proteins*. 2014;82(11):2970-2981.
26. McCarthy AN, Grigera JR. Effect of pressure on the conformation of proteins. A molecular dynamics simulation of lysozyme. *J Mol Graph Model*. 2006;24(4):254-261.
27. Buchner J, Kiefhaber T. *Protein Folding Handbook*. 2005. p.
28. Kitchen DB, Reed LH, Levy RM. Molecular dynamics simulation of solvated protein at high pressure. *Biochem US*. 2002;31(41):10083-10093.
29. Espinosa YR, Grigera JR, Caffarena ER. Essential dynamics of the cold denaturation: pressure and temperature effects in yeast frataxin. *Proteins*. 2017;85(1):125-136.
30. Marchi M, Akasaka K. Simulation of hydrated BPTI at high pressure: changes in hydrogen bonding and its relation with NMR experiments. *J Phys Chem B*. 2001;105(3):711-714.
31. Sarma R, Paul S. Trimethylamine-N-oxide's effect on polypeptide solvation at high pressure: a molecular dynamics simulation study. *J Phys Chem B*. 2013;117(30):9056-9066.
32. Lerbret A, Hédoux A, Annighöfer B, Bellissent-Funel M-C. Influence of pressure on the low-frequency vibrational modes of lysozyme and water: a complementary inelastic neutron scattering and molecular dynamics simulation study. *Proteins*. 2013;81(2):326-340.
33. Mori Y, Okamoto Y. Conformational changes of ubiquitin under high pressure conditions: a pressure simulated tempering molecular dynamics study. *J Comput Chem*. 2017;38(15):1167-1173.
34. Ji Z, Yu L, Liu H, Bao X, Wang Y, Chen L. Effect of pressure with shear stress on gelatinization of starches with different amylose/amylopectin ratios. *Food Hydrocoll*. 2017;72:331-337.
35. Oh HE, Pinder DN, Hemar Y, Anema SG, Wong M. Effect of high-pressure treatment on various starch-in-water suspensions. *Food Hydrocoll*. 2008;22(1):150-155.
36. Szwengiel A, Lewandowicz G, Gorecki AR, Blaszczak W. The effect of high hydrostatic pressure treatment on the molecular structure of starches with different amylose content. *Food Chem*. 2018;240:51-58.
37. Wei B, Cai C, Jin Z, Tian Y. High-pressure homogenization induced degradation of amylopectin in a gelatinized state. *Starch - Stärke*. 2016;68(7–8):734-741.
38. Li W, Zhang F, Liu P, Bai Y, Gao L, Shen Q. Effect of high hydrostatic pressure on physicochemical, thermal and

morphological properties of mung bean (Vigna radiata L.) starch. *J Food End*. 2011;103(4):388-393.
39. Liu H, Wang L, Cao R, Fan H, Wang M. In vitro digestibility and changes in physicochemical and structural properties of common buckwheat starch affected by high hydrostatic pressure. *Carbohydr Polym*. 2016;144:1-8.
40. Wang J, Zhu H, Li S, Wang S, Wang S, Copeland L. Insights into structure and function of high pressure-modified starches with different crystalline polymorphs. *Int J Biol Macromol*. 2017;102:414-424.
41. Wang P, Jin S, Guo H, Zhao L, Ren F. The pressure-induced, lactose-dependent changes in the composition and size of casein micelles. *Food Chem*. 2015;173:468-474.
42. Dissanayake M, Kasapis S, George P, Adhikari B, Palmer M, Meurer B. Hydrostatic pressure effects on the structural properties of condensed whey protein/lactose systems. *Food Hydrocoll*. 2013;30(2):632-640.
43. Krzyźaniak A, Salański P, Jurczak J, Barciszewski J. B-Z DNA reversible conformation changes effected by high pressure. *FEBS Lett*. 1991;279(1):1-4.
44. Wilton DJ, Ghosh M, Chary KV, Akasaka K, Williamson MP. Structural change in a B-DNA helix with hydrostatic pressure. *Nucleic Acids Res*. 2008;36(12):4032-4037.
45. Takahashi S, Sugimoto N. Effect of pressure on the stability of G-quadruplex DNA: thermodynamics under crowding conditions. *Angew Chem Int Ed*. 2013;52(51):13774-13778.
46. Takahashi S, Sugimoto N. Pressure-dependent formation of i-motif and G-quadruplex DNA structures. *Phys Chem Chem Phys*. 2015;17(46):31004-31010.
47. Takahashi S, Bhowmik S, Sugimoto N. Volumetric analysis of formation of the complex of G-quadruplex DNA with hemin using high pressure. *J Inorg Biochem*. 2017;166:199-207.
48. Rayan G, Macgregor RB Jr. A look at the effect of sequence complexity on pressure destabilisation of DNA polymers. *Biophys Chem*. 2015;199:34-38.
49. Patra S, Anders C, Schummel PH, Winter R. Antagonistic effects of natural osmolyte mixtures and hydrostatic pressure on the conformational dynamics of a DNA hairpin probed at the single-molecule level. *Phys Chem Chem Phys*. 2018;20(19):13159-13170.
50. Rayan G, Macgregor RB Jr. Pressure-induced helix-coil transition of DNA copolymers is linked to water activity. *Biophys Chem*. 2009;144(1–2):62-66.
51. Miner JC, Chen AA, Garcia AE. Free-energy landscape of a hyperstable RNA tetraloop. *P Natl Acad Sci USA*. 2016;113(24):6665-6670.
52. Schuabb C, Pataraia S, Berghaus M, Winter R. Exploring the effects of temperature and pressure on the structure and stability of a small RNA hairpin. *Biophys Chem*. 2017;231:161-166.
53. Amiri AR, Macgregor RB Jr. The effect of hydrostatic pressure on the thermal stability of DNA hairpins. *Biophys Chem*. 2011;156(1):88-95.
54. Giel-Pietraszuk M, Barciszewski J. A nature of conformational changes of yeast tRNA (Phe). High hydrostatic pressure effects. *Int J Biol Macromol*. 2005;37(3):109-114.
55. Schuabb C, Berghaus M, Rosin C, Winter R. Exploring the free energy and conformational landscape of tRNA at high temperature and pressure. *Chem Phys Chem*. 2015;16(1):138-146.
56. Kumar P, Lehmann J, Libchaber A. Kinetics of bulge bases in small RNAs and the effect of pressure on it. *PLoS ONE*. 2012;7(8):e42052.
57. Li H, Yamada H, Akasaka K. Effect of pressure on individual hydrogen bonds in proteins. *Basic Pancreat Trypsin Inhibit Biochem US*. 1998;37(5):1167-1173.
58. Akasaka K. Probing conformational fluctuation of proteins by pressure perturbation. *Chem Rev*. 2006;106(5):1814-1835.
59. Roche J, Royer CA, Roumestand C. Monitoring protein folding through high pressure NMR spectroscopy. *Prog Nucl Mag Res Sp*. 2017;102–103:15-31.
60. Galkin O, Buchter S, Tabirian A, Schulte A. Pressure effects on the proximal heme pocket in myoglobin probed by Raman and near-infrared absorption spectroscopy. *Biophys J*. 1997;73(5):2752-2763.
61. Akasaka K, Kitahara R, Kamatari YO. Exploring the folding energy landscape with pressure. *Arch Biochem Biophys*. 2013;531(1–2):110-115.
62. Lerch MT, Horwitz J, McCoy J, Hubbell WL. Circular dichroism and site-directed spin labeling reveal structural and dynamical features of high-pressure states of myoglobin. *P Natl Acad Sci USA*. 2013;110(49):4714-4722.
63. Nagata Y, Takeda R, Suginome M. High-pressure circular dichroism spectroscopy up to 400 MPa using polycrystalline yttrium aluminum garnet (YAG) as pressure-resistant optical windows. *RSC Adv*. 2016;6(111):109726-109729.
64. Yang C, Jang S, Pak Y. A fully atomistic computer simulation study of cold denaturation of a beta-hairpin. *Nat Commun*. 2014;5:5773.
65. Georgoulia PS, Glykos NM. Molecular simulation of peptides coming of age: accurate prediction of folding, dynamics and structures. *Arch Biochem Biophys*. 2019;664:76-88.
66. Case DA, Ben-Shalom IY, Brozell SR, Cerutti DS, Cheatham TE, III, , Cruzeiro VWD, Darden TA, Duke RE, Ghoreishi D, Gilson MK, Gohlke H, Goetz AW, Greene D, Harris R, Homeyer N, Izadi S, Kovalenko A, Kurtzman T, Lee TS, LeGrand S, Li P, Lin C, Liu J, Luchko T, Luo R, Mermelstein DJ, Merz KM, Miao Y, Monard G, Nguyen C, Nguyen H, Omelyan I, Onufriev AV, Pan F, Qi R, Roe DR, Roitberg A, Sagui C, Schott-Verdugo S, Shen J, Simmerling CL, Smith J, Salomon-Ferrer R, Swails J, Walker RC, Wang J, Wei H, Wolf RM, Wu X, Xiao L, York DM, Kollman PA. AMBER 2018. University of California, San Francisco; 2018.
67. Group W. GLYCAM Web. Complex Carbohydrate Research Center, University of Georgia, Athens, GA; 2005-2019.
68. Maier JA, Martinez C, Kasavajhala K, Wickstrom L, Hauser KE, Simmerling CL. ff14SB: improving the accuracy of protein side chain and backbone parameters from ff99SB. *J Chem Theory Comput*. 2015;11(8):3696-3713.
69. Perez A, Marchan I, Svozil D, et al. Refinement of the AMBER force field for nucleic acids: improving the description of alpha/gamma conformers. *Biophys J*. 2007;92:3817-3829.
70. Zgarbova M, Otyepka M, Sponer J, et al. Refinement of the Cornell et al. nucleic acids force field based on reference quantum chemical calculations of glycosidic torsion profiles. *J Chem Theory Comput*. 2011;7(9):2886-2902.
71. Kirschner KN, Yongye AB, Tschampel SM, et al. GLYCAM06: A generalizable biomolecular force field. *Carbohydrates J Comput Chem*. 2008;29(4):622-655.

72. Grossfield A. n.d. WHAM: the weighted histogram analysis method. 2.0.9.
73. Sims GE, Kim SH. Global mapping of nucleic acid conformational space: dinucleoside monophosphate conformations and transition pathways among conformational classes. *Nucleic Acids Res*. 2003;31(19):5607-5616.
74. Åqvist J, Wennerström P, Nervall M, Bjelic S, Brandsdal BO. Molecular dynamics simulations of water and biomolecules with a Monte Carlo constant pressure algorithm. *Chem Phys Lett*. 2004;384(4–6):288-294.
75. Izaguirre JA, Catarello DP, Wozniak JM, Skeel RD. Langevin stabilization of molecular dynamics. *J Chem Phys*. 2001;114(5):2090-2098.
76. Frisch MJ, Trucks GW, Schlegel HB, Scuseria GE, Robb MA, Cheeseman JR, Scalmani G, Barone V, Petersson GA, Nakatsuji H, Li X, Caricato M, Marenich AV, Bloino J, Janesko BG, Gomperts R, Mennucci B, Hratchian HP, Ortiz JV, Izmaylov AF, Sonnenberg JL, Williams-Young D, Ding F, Lipparini F, Egidi F, Goings J, Peng B, Petrone A, Henderson T, Ranasinghe D, Zakrzewski VG, Gao J, Rega N, Zheng G, Liang W, Hada M, Ehara M, Toyota K, Fukuda R, Hasegawa J, Ishida M, Nakajima T, Honda Y, Kitao O, Nakai H, Vreven T, Throssell K, Montgomery Jr. JA, Peralta JE, Ogliaro F, Bearpark MJ, Heyd JJ, Brothers EN, Kudin KN, Staroverov VN, Keith TA, Kobayashi R, Normand J, Raghavachari K, Rendell AP, Burant JC, Iyengar SS, Tomasi J, Cossi M, Millam JM, Klene M, Adamo C, Cammi R, Ochterski JW, Martin RL, Morokuma K, Farkas O, Foresman JB, Fox DJ. Gaussian 16 Rev. C.01. Wallingford, CT; 2016.
77. Becke AD. Density-functional thermochemistry. III. The role of exact exchange. *J Chem Phys*. 1993;98(7):5648-5652.
78. Grimme S, Ehrlich S, Goerigk L. Effect of the damping function in dispersion corrected density functional theory. *J Comput Chem*. 2011;32(7):1456-1465.
79. Barone V, Cossi M. Quantum calculation of molecular energies and energy gradients in solution by a conductor solvent model. *J Phys Chem A*. 1998;102(11):1995-2001.
80. Jungwirth J, Šebestík J, Šafařík M, Kapitán J, Bouř P. Quantitative determination of Ala-Ala conformer ratios in solution by decomposition of Raman optical activity spectra. *J Phys Chem B*. 2017;121(38):8956-8964.
81. Roe DR, Cheatham TE III. PTRAJ and CPPTRAJ: software for processing and analysis of molecular dynamics trajectory data. *J Chem Theory Comput*. 2013;9(7):3084-3095.
82. Bouř P, Keiderling TA. Partial optimization of molecular geometry in normal coordinates and use as a tool for simulation of vibrational spectra. *J Chem Phys*. 2002;117(9):4126-4132.
83. Bouř P. Convergence properties of the normal mode optimization and its combination with molecular geometry constraints. *Collect Czech Chem C*. 2005;70(9):1315-1340.
84. Qgrad BP. *Institute of Organic Chemistry and Biochemistry*. Prague, Czech Republic: Academy of Sciences; 2006.
85. Onufriev AV, Izadi S. Water models for biomolecular simulations. *Wires Comput Mol Sci*. 2018;8(2):e1347.
86. Best RB, Miller C, Mittal J. Role of solvation in pressure-induced helix stabilization. *J Chem Phys*. 2014;141(22):22D522.
87. Anandakrishnan R, Izadi S, Onufriev AV. Why computed protein folding landscapes are sensitive to the water model. *J Chem Theory Comput*. 2019;15(1):625-636.
88. Gupta M, Nayar D, Chakravarty C, Bandyopadhyay S. Comparison of hydration behavior and conformational preferences of the Trp-cage mini-protein in different rigid-body water models. *Phys Chem Chem Phys*. 2016;18(48):32796-32813.
89. Dukor RK, Keiderling TA. Reassessment of the random coil conformation: vibrational CD study of proline oligopeptides and related polypeptides. *Biopolymers*. 1991;31(14):1747-1761.
90. Hermans J. The amino acid dipeptide: small but still influential after 50 years. *P Natl Acad Sci USA*. 2011;108(8):3095-3096.
91. Takeyiko T, Imai T, Kato M, Taniguchi Y. Temperature and pressure effects on conformational equilibria of alanine dipeptide in aqueous solution. *Biopolymers*. 2004;73(2):283-290.
92. Okumura H, Okamoto Y. Temperature and pressure dependence of alanine dipeptide studied by multibaric–multithermal molecular dynamics simulations. *J Phys Chem B*. 2008;112(38):12038-12049.
93. Vymětal J, Vondrášek J. Metadynamics as a tool for mapping the conformational and free-energy space of peptides – the alanine dipeptide case study. *J Phys Chem B*. 2010;114(16):5632-5642.
94. Takekiyo T, Yoshimura Y, Okuno A, Kato M, Taniguchi Y. Pressure-induced amide I′ frequency shift of model compound of proteins in water. Proceedings of the 4th International Conference on High Pressure Bioscience and Biotechnology 2007;1:47–52.
95. Akasaka K, Matsuki H. *High Pressure Bioscience*. Dordrecht: Springer; 2015:730.

How to cite this article: Plamitzer L, Bouř P. Pressure dependence of vibrational optical activity of model biomolecules. A computational study. *Chirality*. 2020;32:710–721. https://doi.org/10.1002/chir.23216